Wear 580-581 (2025) 206292

Contents lists available at ScienceDirect

Wear

journal homepage: www.elsevier.com/locate/wear

Grey-box modelling for tool wear prediction in milling: Fusion of finite element insights, time-resolved cutting signals and metaheuristic feature selection

Amirmohammad Jamali [a], Amod Kashyap [b,c,*], Johannes Schneider [b,c], Michael Stueber [d], Volker Schulze [a]

[a] Institute of Production Science (wbk), Karlsruhe Institute of Technology, Karlsruhe, 76131, Germany
[b] Institute of Applied Materials (IAM-ZM), Karlsruhe Institute of Technology, Karlsruhe, 76131, Germany
[c] Micro-Tribology Centre (μTC), Karlsruhe Institute of Technology, Karlsruhe, 76131, Germany
[d] Institute of Applied Materials (IAM-AWP), Karlsruhe Institute of Technology, Karlsruhe, 76131, Germany

ARTICLE INFO

Keywords:
Tool wear prediction
Grey-box modelling
Finite element simulation
Machine learning in manufacturing

ABSTRACT

Reliable prediction of tool wear is essential for ensuring productivity, quality, and cost-efficiency in modern machining operations. This study presents a hybrid Grey-Box machine learning framework that combines White-Box finite element simulation outputs (interface temperature, relative sliding velocity), process parameters (feed speed, cutting velocity, depth of cut), dynamic time-series features from cutting force measurements, with a Black-Box machine learning model to predict tool wear in high-speed milling. The experimental campaign involved TiN-coated and uncoated carbide tools under dry machining conditions, with flank and rake wear measured after each cutting pass. Finite element simulations were conducted to extract localized thermo-mechanical features, such as interface temperature and relative sliding velocity, which were used as physically meaningful inputs. A two-step feature selection method—based on analysis of variance (ANOVA) and the whale optimization algorithm (WOA)—was employed to identify the most relevant input features. Among the machine learning models tested, the gradient boosting regressor (GBR) showed the highest accuracy, achieving coefficient of determination (R^2) scores of 0.953 for rake wear and 0.920 for flank wear. Omitting White-Box features resulted in significantly lower performance, confirming their critical role. The model's predictions were also in line with the unseen test cases. These results highlight the effectiveness of combining simulation-informed features with empirical data for tool condition monitoring, offering a scalable and interpretable approach for predictive maintenance in smart manufacturing.

1. Introduction

Machining is a fundamental process in modern manufacturing, enabling the production of high-precision components across critical industries such as automotive, aerospace, and medical devices [1–5]. One of the major challenges in machining is tool wear, which directly affects surface quality, dimensional accuracy, process stability, and productivity. If not adequately predicted, wear can lead to sudden tool failure, increased scrap rates, and costly downtime [6–8].

As manufacturing advances toward Industry 4.0, there is increasing emphasis on intelligent tool condition monitoring systems that support predictive maintenance. These systems aim to detect wear evolution in real time and optimize tool usage through data-driven insights [9,10]. In this context, hybrid models (integrating physical modelling and machine learning) are gaining attention for their ability to provide interpretable and accurate wear predictions under varying process conditions [11–13].

Traditional methods, such as Taylor's tool life equation, offer only limited predictive capability due to their dependence on controlled conditions and simplified assumptions. Similarly, manual inspection-based approaches remain widely used but are subjective and cannot reliably capture the progression of wear [1,5]. With increasing

This article is part of a special issue entitled: Grey Box Wear Prediction_invited only published in Wear.

* Corresponding author. Institute of Applied Materials (IAM-ZM), Karlsruhe Institute of Technology, Karlsruhe, 76131, Germany.
E-mail address: amod.kashyap@kit.edu (A. Kashyap).

https://doi.org/10.1016/j.wear.2025.206292
Received 10 June 2025; Received in revised form 7 August 2025; Accepted 14 August 2025
Available online 16 August 2025

computational resources, Black-Box models using data-driven techniques have become popular due to their potential for rapid, flexible predictions. However, these models often require large quantities of experimental data and offer limited transparency [14].

To overcome these challenges, Grey-Box approaches aim to merge the strengths of physics-based (White-Box) models with data-driven (Black-Box) learning. In cases where process understanding exists, even a limited set of experimental results can be enriched with simulations (such as finite element analysis) to create powerful predictive models [15–17]. Still, existing modelling strategies often fall short in capturing multi-scale wear mechanisms, particularly those involving coated tools. Phenomena like coating delamination and microstructural degradation remain difficult to simulate without excessive computational cost [18–21].

Recent research has demonstrated promising developments. Researchers have introduced an FE-based model, which used a modified Usui equation, to simulate dynamic wear [14,22–24]. Sensor-based studies have shown that cutting forces, vibrations, and acoustic emissions are effective signals for capturing tool condition in real time [8,25,26]. Furthermore, deep learning architectures such as convolutional neural networks (CNNs), gated recurrent units (GRUs), and Transformers have been employed to extract complex patterns from these signals [27,28]. Hybrid approaches, such as physics-informed neural networks and models using physical pseudo-labels, further demonstrate the potential of combining physical knowledge with AI.

Despite significant advances in tool wear prediction, most existing models are limited by their reliance on a single modality either physics-based modelling or sensor-derived data. This narrow focus restricts their ability to generalize across varying tools, coatings, and workpiece materials. Addressing this critical limitation, recent research increasingly calls for integrated modelling strategies that can bridge the gap between multi-scale physical phenomena and complex, real-world data streams.

In response to this challenge, the present study introduces a novel Grey-Box machine learning framework for predicting tool wear in milling operations. Uniquely, the proposed model fuses simulation-based thermomechanical features, process parameters, and time-resolved force signals into a cohesive predictive architecture. To enhance both model accuracy and interpretability, a two-stage feature selection strategy (combining ANOVA and the Whale Optimization Algorithm (WOA)) is employed to extract the most informative input features. In the previous research, the authors discussed the use of ANOVA + WOA for feature selection and its importance [7]. It was found that ANOVA + WOA in conjunction with support vector machine (SVM) gave a better classification quality. This combination ensured that only the most relevant features, those with high discriminative power, were selected, thereby enhancing the accuracy of the classification model. The superiority of this approach was particularly evident in scenarios with imbalanced or noisy data, where traditional methods struggled to maintain performance. However, in the present article, the authors have gone one step further: Here, they use the same two-stage feature selection (ANOVA + WOA), but within the framework of a regression model to precisely predict the wear values (flank and rake wear). In addition, they have also combined the data-based features from the force signals with physically sound simulation results (Grey--Box approach). The model was trained with several regression methods (support vector regression (SVR) and GBR), with GBR delivering the best results. Thus, this article aims not only to distinguish classes but also to predict concrete wear values. The novelty lies in the specific fusion of physics-based FEM features (e.g., temperature, sliding velocity) with empirical, time-resolved force signal processing for tool wear prediction under industrial high-speed milling conditions.

The significance of this work lies not only in its technical innovation but also in its potential impact on industrial practice. By integrating multi-source data and hybrid modelling approaches, this research contributes a generalizable, physically grounded, and data-efficient solution for intelligent tool condition monitoring. Ultimately, the proposed framework represents a key step toward reliable, real-time, and autonomous decision-making in next-generation manufacturing systems.

2. Materials and methods

2.1. Purpose of the experiments

The purpose of the present investigation was to systematically examine the effects of cutting parameters and tool coating on the wear of flank and rake face during dry milling. In order to create Grey-Box models that can forecast tool wear, the goal was to produce high-quality data for the machining of AISI 1045 steel under carefully monitored circumstances. This article aims to close the gap between simulation-based and purely empirical wear prediction models by integrating measured cutting forces with wear observations and physical insights.

2.2. Tool and workpiece materials

The experiments were carried out using indexable cutting inserts of two types, titanium nitride (TiN) coated and uncoated. Both variants were based on a cemented carbide substrate with hard tungsten carbide (WC) particles in the matrix of 10 wt% of cobalt (Co). The TiN coating had a thickness of approximately 5 μm estimated from a cross-sectional sample prepared by using dual beam focused ion beam (FIB), scanning electron microscope (Helios NanoLab Dualbeam 650, ThermoFisher, USA), Fig. 1(a). The material used for the workpiece was normalized AISI 1045 carbon steel, with dimensions of 100 mm × 100 mm × 150 mm. Fig. 1(b) shows the microstructure of the normalized AISI 1045 carbon steel having fine-grained mixture of ferrite and pearlite. All machining operations were carried out on a POSmill CE 1000 machine (POS, Germany).

The inserts used were uncoated CCHT 6682 (Gühring®, Germany) and TiN-coated CCHT 6684 (Gühring®, Germany) (Fig. 2). The cutting velocities used for the machining experiments were 112 and 132 m/min.

The cutting-edge radius measured 0.035 mm for the uncoated insert and 0.045 mm for the coated one. The clearance angle was set at 7°, while the rake angle was 10° across all inserts. All milling operations were carried out under dry conditions without any lubrication, mimicking realistic industrial scenarios for dry machining.

2.3. Cutting conditions

The cutting experiments aimed to investigate different cutting intensities by adjusting the cutting velocity and feed speed, while keeping the axial and radial depths of cut consistent. Table 1 lists the 12 cases examined. In each case, the axial depth of cut a_p was fixed at 2 mm, and the radial depth of cut a_e at 0.5 mm. The cutting velocity and feed speed varied across the different cases, along with the tool coating condition, which was either TiN or uncoated. Although this study investigated 12 process parameter conditions, each was evaluated in triplicate, and wear progression was sampled over multiple cutting passes, resulting in a robust time-series dataset for model development. Therefore, the total number of samples or records generated for one experiment with N cutting passes will be the product of N cutting passes, 3 repeats, and 12 process parameters.

2.4. Force and wear measurement

Cutting force measurements were captured using a piezoelectric three-component dynamometer (9257B, Kistler®, Germany), mounted rigidly between the workpiece and the machine table. The system included a charge amplifier and was operated at a sampling rate of 10 kHz to ensure accurate dynamic force acquisition.

Tool wear was measured ex-situ using a digital light microscope (VHX 6000, Keyence®, Japan) after every 150 mm of cutting path. The

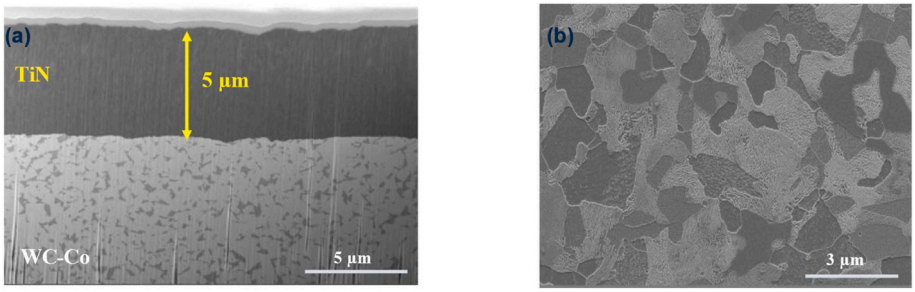

Fig. 1. SEM image of (a) FIB prepared cross-section of the coating, (b) microstructure of the normalized AISI 1045 carbon steel.

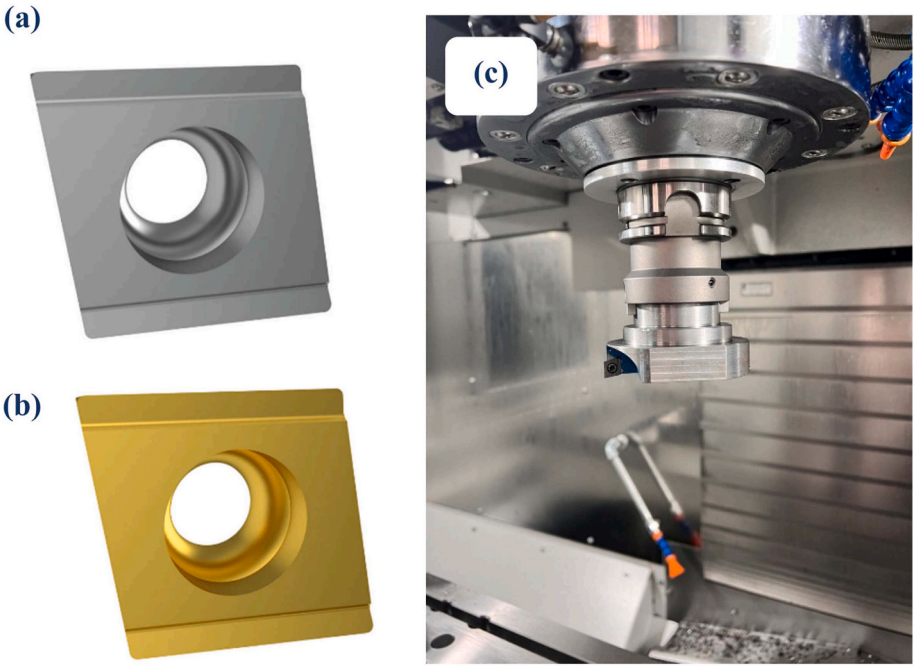

Fig. 2. a) Gühring® CCHT 6682 (uncoated), b) CCHT 6684 (TiN-coated) insert and c) cutting tool holder.

Table 1
Cutting parameters used for the experimental investigation (3 individual tests per case).

Case number	Coating	a_p mm	a_e mm	v_c m/min	v_f mm/min
1	TiN	2 mm	0.5	112	200
2	TiN	2 mm	0.5	132	200
3	TiN	2 mm	0.5	112	250
4	TiN	2 mm	0.5	132	250
5	TiN	2 mm	0.5	112	150
6	TiN	2 mm	0.5	132	150
7	Uncoated	2 mm	0.5	112	200
8	Uncoated	2 mm	0.5	132	200
9	Uncoated	2 mm	0.5	112	150
10	Uncoated	2 mm	0.5	132	150
11	Uncoated	2 mm	0.5	112	250
12	Uncoated	2 mm	0.5	132	250

tool wear defined in the present investigation is the width of wear scar on the flank and the rake face. Both flank wear (VB) and rake face wear (KT) were recorded for each tooth. The measured values were further used for analysis and model training.

To ensure repeatability and reduce the standard deviation, all 12 experimental conditions were performed three times. The resulting data were averaged, and standard deviations were calculated to appropriately capture the trends in the wear behavior.

All tests were carried out in a dry machining environment to eliminate the effects of lubrication and focus solely on thermal and mechanical interactions between tool and workpiece.

2.5. White-Box (simulation) approach

To support the experimental findings and extract physically relevant insights, a two-dimensional orthogonal milling simulation was carried out using the commercial finite element softwareMSC Marc (Hexagon AB, Sweden), together with its pre- and post-processor MENTAT (Hexagon AB, Sweden). The simulation employs an updated Lagrangian approach and features an automatic remeshing function that triggers in response to local strain developments. To ensure the accuracy of the results, remeshing was limited to a rate that preserves element quality without relying too heavily on interpolation, since excessive remeshing can lead to numerical instability [29].

In this study, the finite element simulations are conducted with the unworn tool geometry as the initial condition. Consequently, the FEM models do not account for geometry updates, edge rounding, or contact condition evolution that develop as the tool wears during machining. As a result, the extracted thermomechanical features (e.g., maximum interface temperature, sliding velocity) are representative of the initial tool condition for each process parameter set, rather than continuously evolving with wear.

2.5.1. Model geometry and boundary conditions

The simulation model is composed of six primary components: the cutting insert, a TiN coating layer, the elasto-plastic region of the workpiece, an elastic zone beneath the elasto-plastic region of the workpiece, and individual holders for both the tool and the workpiece (Fig. 3). Together, the elastic and elasto-plastic regions represent the full structure of the workpiece. To ensure consistency with the experimental setup, the cutting insert was modelled using the exact geometry used in testing, including both the coating and the substrate layers.

Boundary conditions were applied to the workpiece and the cutting tool holders. The tool holder was responsible for imposing the rotational speed of the insert and maintaining a thermal boundary condition of 25 °C. Similarly, the workpiece holder controlled its translational movement and also maintained a 25 °C thermal boundary at the interface. All simulations were conducted under dry cutting conditions, mimicking the experimental configuration. Environmental heat exchange was captured using a convective heat transfer coefficient of 50 W/(m^2·K), which aligns with values commonly reported for dry machining scenarios [30].

2.5.2. Meshing and material zones

A structured hexagonal mesh was used to model both the cutting tool and its coating. To accurately capture thermal and mechanical gradients, adaptive mesh refinement was implemented, with the smallest element edge length set to 1 μm in the critical areas, particularly at the chip–coating interface. The workpiece was divided into two distinct zones: a deformable elasto-plastic region near the cutting area, and a surrounding elastic region. This two-zone strategy was adopted to balance computational efficiency while accurately modelling the physics, like effective modelling of stress wave propagation and heat transfer beyond the main deformation zone. Remeshing was restricted to the elasto-plastic region, where large strains and deformations are concentrated.

2.5.3. Workpiece material model

The material behavior of the AISI 1045 steel workpiece was modelled as temperature-dependent, using experimentally validated data from the literature. Plastic deformation within the cutting zone was represented using the Johnson–Cook constitutive model, a well-established approach for simulating high-strain-rate processes like machining. The equivalent flow stress, σ_f, is determined using the following expression:

$$\sigma_f = [A + B(\bar{\varepsilon})^n]\left[1 + C\ln\left(\frac{\dot{\varepsilon}}{\dot{\epsilon_0}}\right)\right]\left[1 - \left(\frac{T - T_0}{T_m - T_0}\right)^m\right] \quad (1)$$

In this expression, $\bar{\varepsilon}$ is the equivalent plastic strain, $\dot{\varepsilon}$ is the plastic strain rate, and $\dot{\epsilon_0}$ is the reference strain rate. T represents the current temperature, T_0 is the ambient (room) temperature, and T_m is the melting temperature of the material. The model parameters A, B, C, n, and m were selected based on values reported in previous machining simulation studies and are summarized in Table 2 [31].

In addition to the heat generated by plastic deformation, a conversion factor of 90 % was applied to the plastic work to simulate heat generation within the shear zone. This approach follows the recommendation of [26] and is further supported by metal cutting studies conducted by Refs. [31,32].

2.5.4. Cutting tool and coating properties

The thermal and mechanical properties of the cemented carbide cutting tool were assumed to be temperature-independent for simplification purposes, with reference values taken at 25 °C. These properties are listed in Table 3 [33].

For the TiN coating, essential material parameters such as thermal conductivity λ, specific heat C_p, density ρ, Thermal expansion coefficient α_r and elastic modulus E were sourced from validated literature [34]. These values are presented in Table 4. The coating was modelled with perfect adhesion to the substrate, and no interfacial defects or imperfections were considered in the simulation.

2.5.5. Contact and friction model, thermal contact and heat transfer

Accurate modelling of the tool–workpiece interface is critical to the reliability of orthogonal cutting simulations, especially when aiming to predict coupled thermal and mechanical behaviours. In this study, contact is established between the TiN-coated/uncoated surface of the

Table 2
Johnson cook Parameter AISI 1045.

A (MPa)	B (MPa)	C (–)	*n* (–)	*m* (–)
646.19	517.7	0.0102	0.24597	0.94054

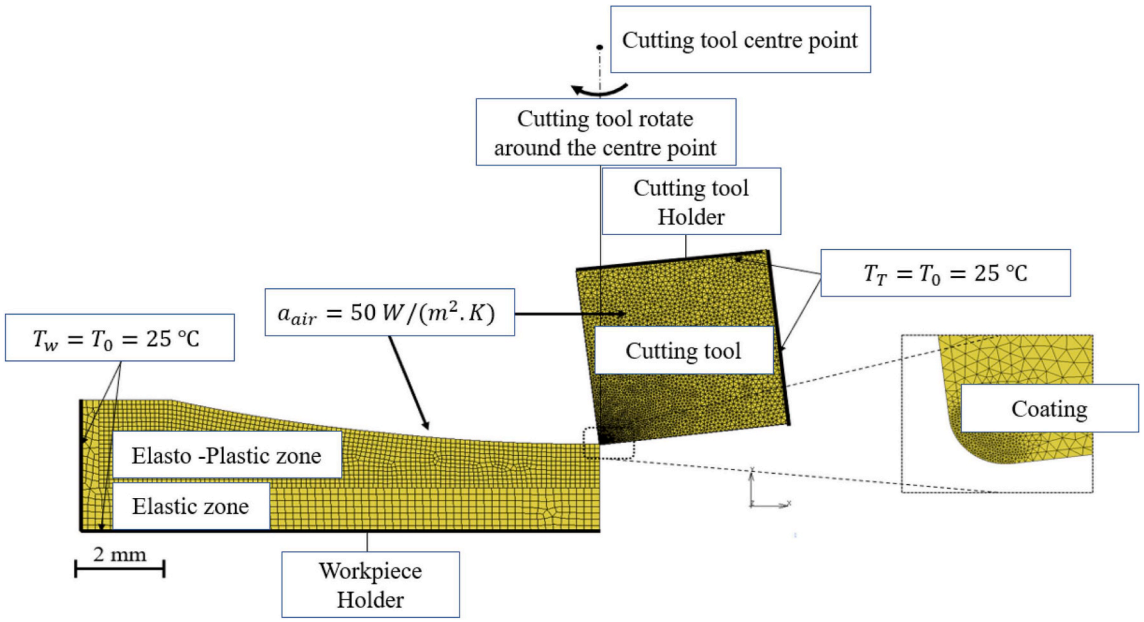

Fig. 3. Simulation setup.

Table 3
Thermo-physical properties of cemented carbide at 25 °C.

λ (W/mK)	C_p (J/Kg.K)	ρ (g/cc)	E (MPa)	α_r (K^{-1})
80	180.54	15.7	7.17E+5	5.5E-6

Table 4
Material properties of the TiN coating at 25 °C.

λ (W/mK)	C_p (J/Kg.K)	ρ (g/cc)	E (MPa)	α_r (K^{-1})
21.0	702.6	5.42	2.5E5	9.35E-06

cutting insert and the AISI 1045 steel workpiece.

To simulate the interaction between the tool and the workpiece, a pressure-dependent Coulomb friction model was used, as shown in Eq. (2), where the friction coefficient (μ) and the shear stress (k) depend on the normal stresses (σ_n) applied to the contact, and therefore the frictional stress (τ_f) between the tool and the workpiece [35]. This approach accounts for changes in contact behavior based on the local pressure at the interface. When the contact pressure is below the yield strength of the workpiece material, friction is described using a variable friction coefficient that increases with pressure. If the pressure exceeds the material's yield strength, a limiting shear stress is applied instead. This method offers a more realistic representation of friction under different loading conditions [35]. The coefficients are directly taken from the previous work done at our lab by Holey et al. [23] and Sauer et al. [33], where they were derived using a multiscale simulation approach incorporating contact mechanics and atomistic simulations (DFT-MD). In the present work, the authors have used these values as a forward modelling strategy without further tuning, as the focus was on evaluating the influence of physically motivated chip formation parameters, and not on adjusting friction behavior itself.

$$\tau_f(\sigma_n) = \begin{cases} \mu(\sigma_n), \sigma_n < \sigma_Y \\ k(\sigma_n), \sigma_n \geq \sigma_Y \end{cases} \quad (2)$$

in addition to frictional effects, thermal conductivity at the tool–chip interface plays a key role in accurately predicting temperature distribution during cutting. To model heat transfer between the TiN coating and the AISI 1045 steel workpiece, a constant heat transfer coefficient was applied at the contact surface. Based on recent research at the institute [29], the heat transfer coefficient was set to a value of 50 W/m^2K. This choice ensures a realistic representation of heat dissipation between the chip and the coated surface of the cutting insert.

The simulations were performed using a 2D orthogonal milling model in MARC MENTAT software, incorporating a TiN-coated carbide tool and an AISI 1045 steel workpiece. Cutting parameters (e.g. feed speed (v_f), cutting velocity (v_c), and environmental temperature, etc.) matched the experimental setup. The finite element simulation offers localized insights that are difficult to capture experimentally but are essential for understanding the thermal and tribological mechanisms contributing to tool wear. For each simulated case, three key physical quantities were extracted position-dependent along the tool–chip contact zones:

- Temperature distribution
- Normal contact stress
- Relative sliding velocity

Usui et al. also discussed the importance of these physical quantities in his investigation for the prediction of cutting tool wear [36]. These variables were evaluated separately for both the rake face and the flank face of the cutting tool. The extracted temperature and sliding velocity data serve as physically meaningful "White-Box" features for use in the subsequent Grey-Box machine learning model for the prediction of wear.

2.6. Experimental data acquisition

This set includes directly measured parameters from the machining process through various sensors. For each experimental case, cutting force signals in the x, y, and z directions (f_x, f_y, f_z) were recorded over successive cutting passes (e.g., Cut 1, Cut 2, …, Cut n). From these time-series signals, 48 time and frequency-domain features were extracted at each step, which include features like: mean force and root mean square (RMS), peak to peak amplitude, signal energy, force gradient, etc.

2.7. Grey-box modelling implementation

To predict tool wear under realistic machining conditions, a Grey-Box machine learning framework was developed by combining both static (Maximum temperature across the contact length of the tool, v_f, v_c, tool (TiN-coated or uncoated), etc.) and time-dependent input features (mean force and root mean square (RMS), peak to peak amplitude, signal energy, force gradient, etc.). This approach blends physics-based understanding with experimental data, striking a balance between interpretability, predictive accuracy, and practical relevance (Fig. 4).

2.7.1. Feature extraction

The input features used in the model are organized into three categories, each capturing a different dimension of the cutting process.

2.7.1.1. Process parameters. These are the measurable and controllable variables that define the cutting conditions in machining operations like v_f, v_c, and the tool (TiN-coated or uncoated).

2.7.1.2. Experimental data. This dataset includes the cutting force signals in the x, y, and z directions (f_x, f_y, f_z).

2.7.1.3. White-Box outputs. These features are extracted from finite element simulations and describe the localized thermomechanical conditions at the tool–chip interface during a single cutting pass. They represent fundamental physical phenomena that drive wear mechanisms such as adhesion, diffusion, and abrasion.

- Maximum temperature at the rake face
- Maximum temperature at the flank face
- Maximum relative sliding velocity (RSV) at the rake face
- Maximum RSV at the flank face

These input features represent physically meaningful variables influencing tool wear. For instance, the maximum interface temperature extracted from finite element simulations reflects the thermal stresses contributing to diffusion and oxidation wear mechanisms. Likewise, the relative sliding velocity captures tribological conditions that influence adhesion and abrasion. Statistical force signal features such as crest factor and kurtosis relate to mechanical instabilities and transient loading events commonly associated with tool degradation. By combining these features, the model integrates multi-scale wear-related phenomena both from physical simulations and in-process measurements.

2.7.2. Model training and feature selection

Prior to model development, two experimental cases.

1. a TiN-coated tool at $v_f = 250$ mm/min, $v_c = 132$ m/min and
2. an uncoated tool at $v_f = 150$ mm/min, $v_c = 112$ m/min

were set aside to serve as independent validation scenarios. The remaining dataset was cleaned to exclude known deviations and then split into input features and target variables: wear of rake and flank face, **VB** and **KT, respectively.**

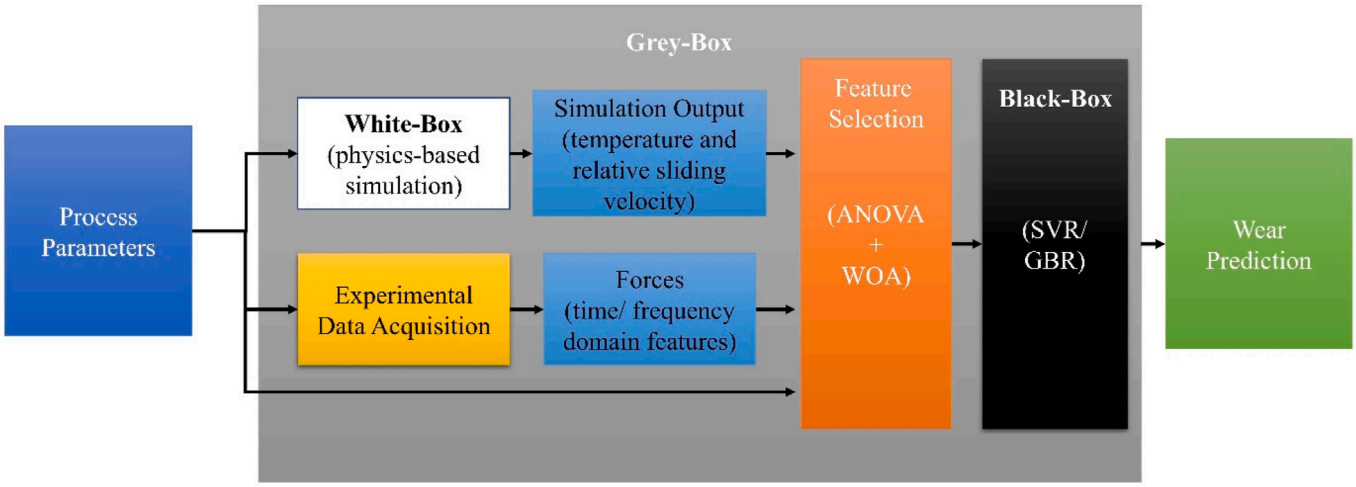

Fig. 4. Schematic representation of the Grey-Box machine learning framework. Physics-based features (White-Box) from finite element simulations are combined with process parameters and experimental data (Black-Box) to train a predictive model for tool wear under realistic machining conditions.

To ensure consistent scaling and accelerate convergence during model training, **z-score normalization** was applied to all input features. An **80:20 random split** was used for training and testing, and **feature selection** was conducted independently for VB and KT. **ANOVA-based feature filtering** was used to identify the top 10 features based on statistical relevance to the target variable.

A **two-stage feature selection** strategy was used to reduce dimensionality and improve interpretability.

1. ANOVA F-score filtering identified the top 10 statistically significant features.
2. These were then refined using the Whale Optimization Algorithm (WOA), a bio-inspired metaheuristic algorithm that mimics the foraging behavior of humpback whales. The optimization objective was to minimize Mean Absolute Error (MAE) over 5-fold cross-validation, promoting robust evaluation of feature subsets. WOA was configured with 30 agents and 50 iterations, balancing exploration depth and computational cost. This process yielded compact, high-quality feature sets that improved generalizability and model interpretability. Empirical findings in recent studies [7] indicate that WOA-based selection improves model accuracy and generalization compared to traditional methods.

Two regression models were trained using the optimized features.

1. **SVR:** A randomized hyperparameter search was performed across kernel types (RBF, polynomial, sigmoid), with tuning of **C, γ (gamma), ε (epsilon),** and **degree** (for polynomial kernels). Model selection used **Repeated K-Fold Cross-Validation (5 folds, 3 repetitions).**
2. **GBR:** The same ANOVA + WOA-based feature selection was used. A randomized search optimized **n_estimators, learning_rate, max_depth,** and **subsample**, again using Repeated K-Fold validation.

2.7.3. *Model architecture and hyperparameter optimization*

To determine the optimal hyperparameter configurations for the SVR and GBR models, the Randomized Search Cross-Validation (RandomizedSearchCV) method from the scikit-learn library was applied. This technique performs stochastic optimization by randomly sampling a fixed number of hyperparameter combinations from a user-defined distribution, making it especially suitable for high-dimensional or computationally expensive models. Compared to exhaustive grid search, this method significantly reduces computation time while still allowing meaningful exploration of the hyperparameter space.

For the SVR model, the following hyperparameters were considered: the regularization parameter C∈{0.1,1,10,100,1000}, the kernel coefficient γ∈{'scale','auto',0.001,0.01,0.1}, the epsilon-insensitive margin ϵ∈{0.01,0.1,1,5}, the kernel function ∈{'rbf','poly','sigmoid'}, and the degree parameter for polynomial kernels ∈{2,3,4} For the GBR model, the tuning process involved the number of boosting stages (n_estimators), the learning rate, the maximum depth of individual trees (max_depth), and the subsample ratio. Specifically, the following value ranges were defined: n_estimators ∈{100,200,300}, learning_rate ∈{0.01,0.05,0.1}, max_depth ∈{3,5,7} and subsample ∈{0.8,1.0}.

The optimization process consisted of sampling 20 hyperparameter combinations (n_iter = 20) from the defined parameter grids. For each sampled combination, the model was trained and validated using Repeated K-Fold Cross-Validation with five splits and two (or three) repetitions. In this method, the dataset is split into five disjoint folds, and the training–validation procedure is repeated multiple times with different random partitions. For each fold, the model is trained on four folds and validated on the remaining one. This helps to mitigate the variability introduced by data partitioning and provides a more stable estimate of model performance. The negative mean squared error (neg-MSE) was used as the evaluation criterion, and the mean value across all repetitions was calculated for each hyperparameter set.

The hyperparameter configuration that achieved the lowest average validation error was selected as optimal. This configuration was then used to retrain the model on the complete training set, and the final model performance was evaluated on a hold-out test set. This systematic approach ensured that the selected model not only achieved good predictive accuracy but also exhibited strong generalization to unseen data.

2.7.4. *Model evaluation and results*

The optimized models were evaluated on a held-out test set (20 % of the data), and performance was measured using mean absolute error (MAE), root mean squared error (RMSE), and **coefficient of determination (R^2),** both on the holdout test sets and the excluded validation conditions. This setup ensures that the models not only fit the training data but also generalize across different tool types and cutting parameters. Both models demonstrated strong predictive accuracy, with high R^2 scores and low error metrics, indicating effective generalization on unseen data.

Additionally, the trained models were tested on the excluded cases (TiN-coated and uncoated tools under specific cutting conditions) to validate generalizability. Predicted wear values were compared against experimental measurements, and prediction trends showed good alignment.

3. Results and analysis

3.1. Tool wear pattern: coated vs. uncoated tools

Tool wear was assessed after each cutting pass by measuring both **rake** and **flank wear** using high-resolution digital light microscopy. The comparative images (Fig. 5) show the wear profiles for TiN-coated and uncoated tools under identical milling conditions (v_f = 200 mm/ min, v_c = 112 m/min). The wear evolution for both rake and flank faces was analysed across multiple machining conditions for coated and uncoated tools (Figs. 6–9). As shown, the coated tool exhibits significantly lower wear depth and smoother wear progression along both the rake and flank faces.

Several key observations can be made.

3.1.1. Influence of tool coating on wear progression

In all cases, the TiN-coated tools consistently showed **slower wear progression** compared to uncoated tools, particularly at higher feed speeds and cutting velocities. This trend is evident in both rake and flank wear plots.

- For instance, at v_f = 250 mm/min, v_c = 132 m/min, the **rake wear of the coated tool** remains below 160 µm throughout the test duration, whereas the **uncoated tool** reaches approximately 220 µm.
- A similar pattern is observed in **flank wear**, where the coated tool remains below 130 µm, while the uncoated tool exceeds 150 µm under the same condition.

This difference can be attributed to the coating's ability to reduce the thermal and mechanical loads transmitted to the tool substrate. The TiN layer minimizes abrasive wear because of its high hardness. Since all the tests conducted in the present study were without any lubrication, high temperatures can be expected at the contact zone. The TiN coatings have a high operating temperature of 600 °C, and they act as thermal barriers, in turn protecting the base material from thermal softening, thereby extending tool life [37].

3.1.2. Rake vs. flank wear behavior

In both tool types, **rake wear progresses faster** than flank wear under identical cutting conditions. This is expected, as the rake face is in direct contact with the hot, high-velocity chip flow, leading to elevated thermal and tribological stresses.

- For example, at v_f = 200 mm/min, v_c = 132 m/min, the **coated tool's rake wear** reaches 150 µm, whereas the **flank wear** is only 115 µm.
- The difference is even more pronounced for uncoated tools, highlighting the critical role of the coating in protecting the rake surface, where thermal and mechanical interactions are more severe.

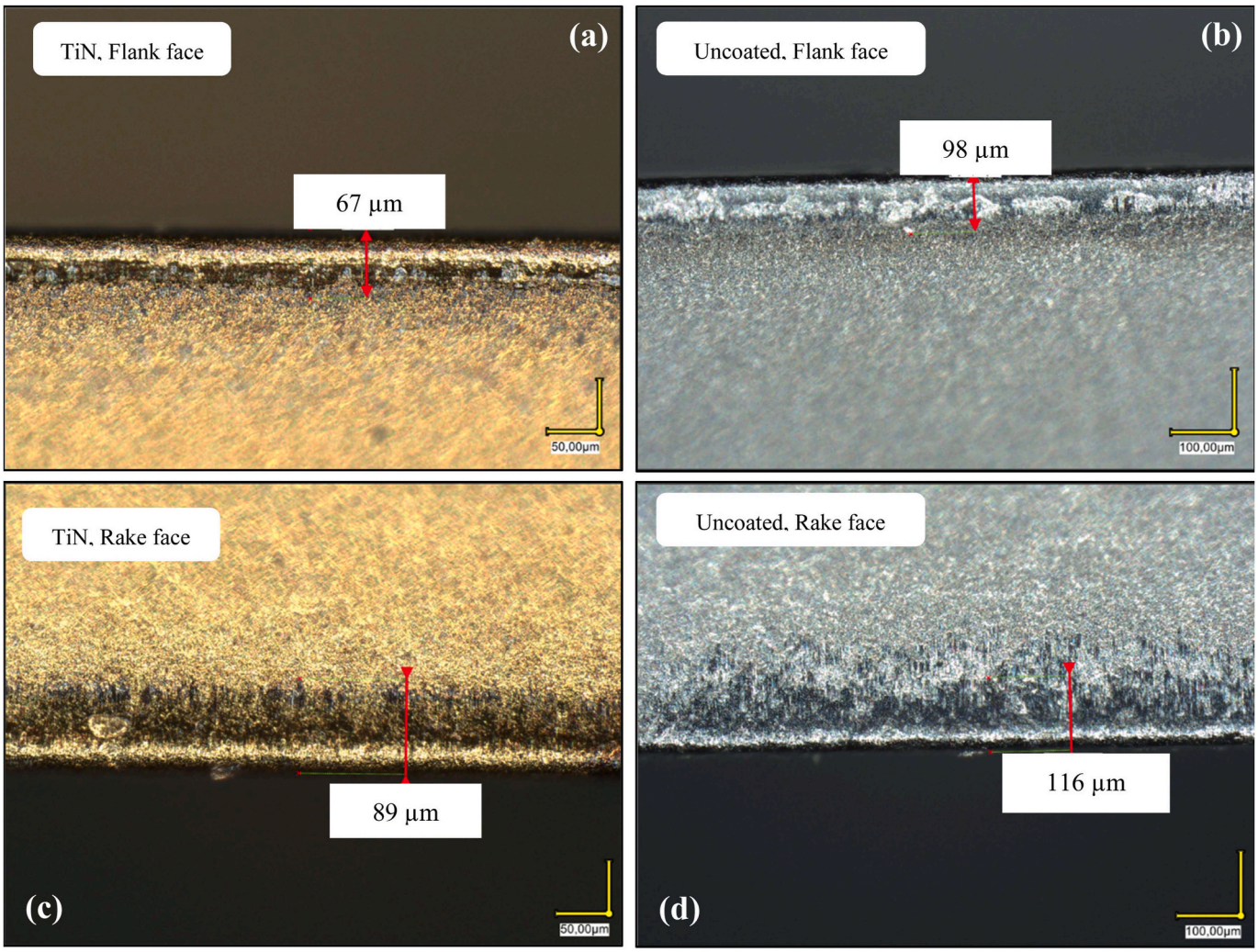

Fig. 5. Microscopic wear patterns at v_f = 200 *mm/min*, n = 850 *rpm* on the flank face (a),(b), and the rake face (c),(d) of TiN-coated and uncoated tools, respectively.

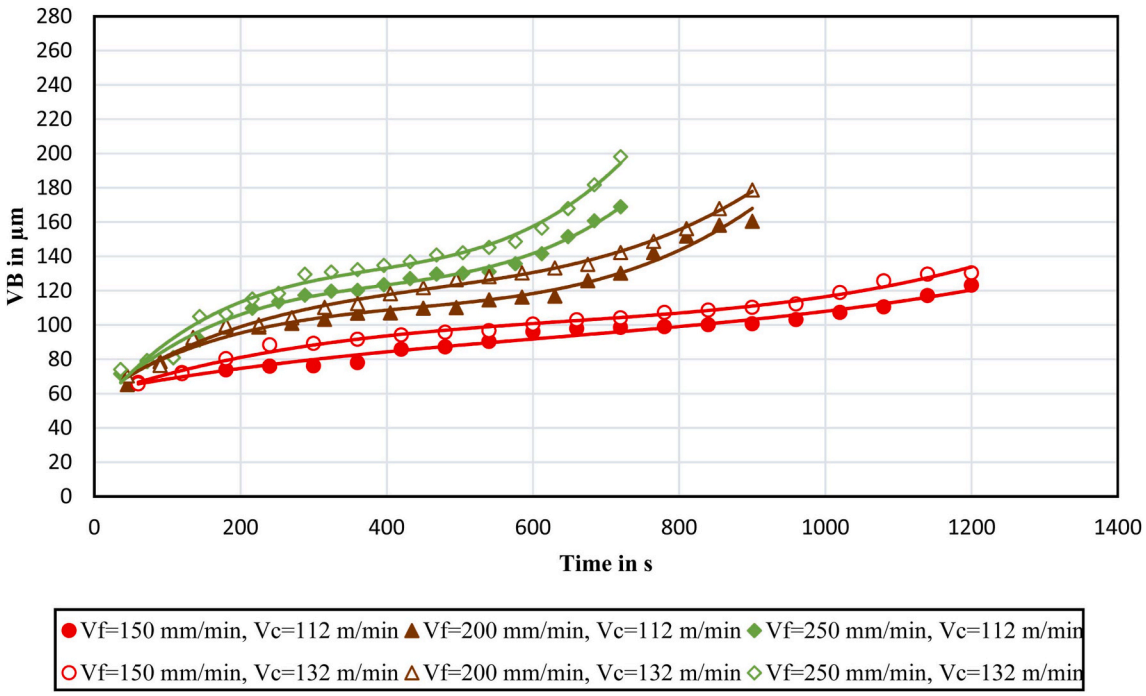

Fig. 6. Wear Progress for Rake face of coated tool.

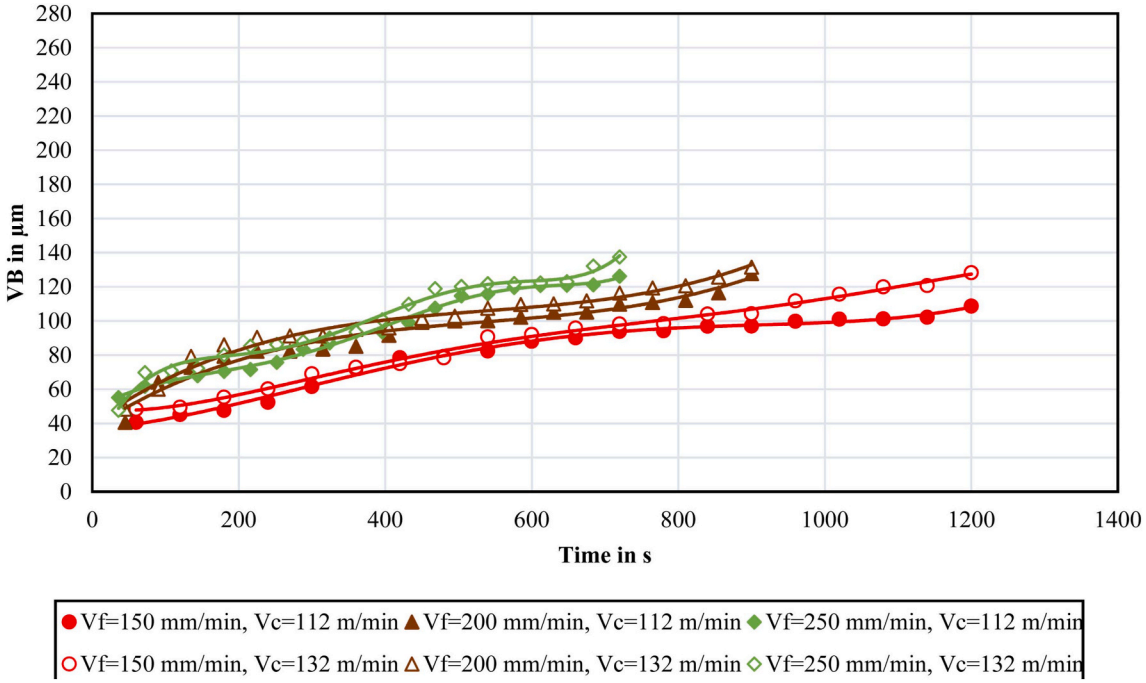

Fig. 7. Wear Progress for Flank face of coated tool.

3.1.3. Effect of cutting parameters

Higher feed speeds and cutting velocities generally correlate with increased wear, regardless of tool coating.

- At higher energy input conditions (e.g., $v_f = 250$ mm/min, $v_c = 132$ m/min), both rake and flank wear accelerate significantly due to higher cutting forces and temperatures.
- Lower-speed conditions (e.g., $v_f = 150$ mm/min, $v_c = 112$ m/ min) result in more moderate wear growth, especially in coated tools, suggesting that the tool–workpiece interaction becomes less severe under reduced thermal and mechanical stress.

3.2. Cutting force progression: coated vs. uncoated tools

To analyze the evolution of cutting forces during the milling process, the raw force signals were processed using **Time Synchronous Averaging (TSA).** This method effectively isolates the periodic components of the cutting force by averaging over repeated spindle revolutions, thereby reducing random noise and improving the signal-to-noise ratio.

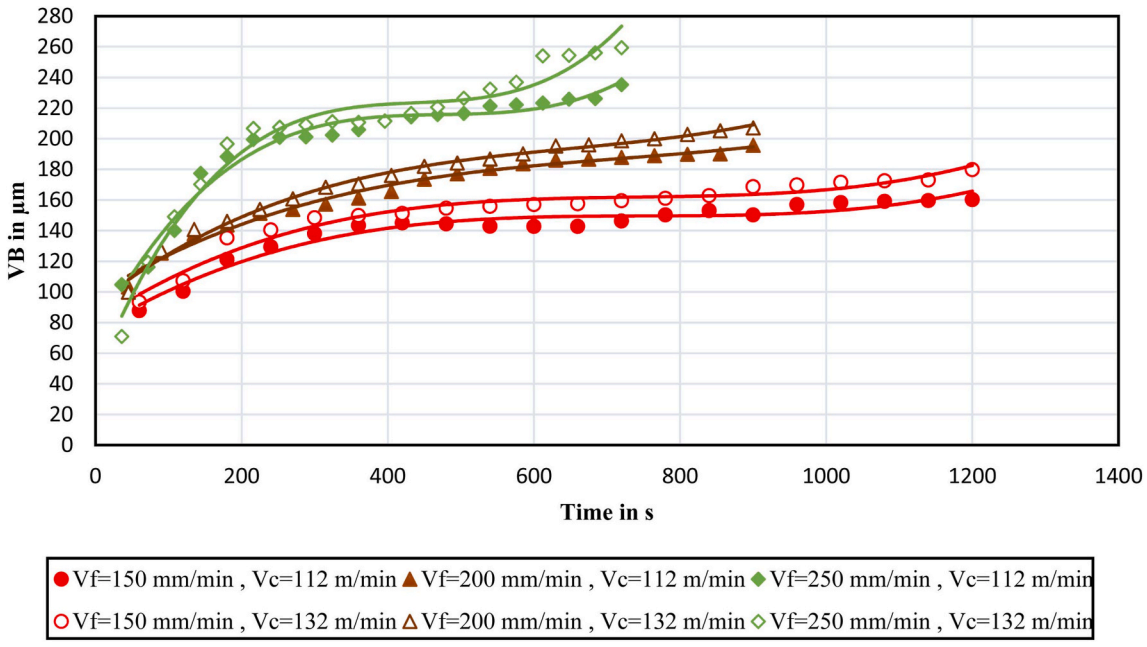

Fig. 8. Wear Progress for Rake face of uncoated tool.

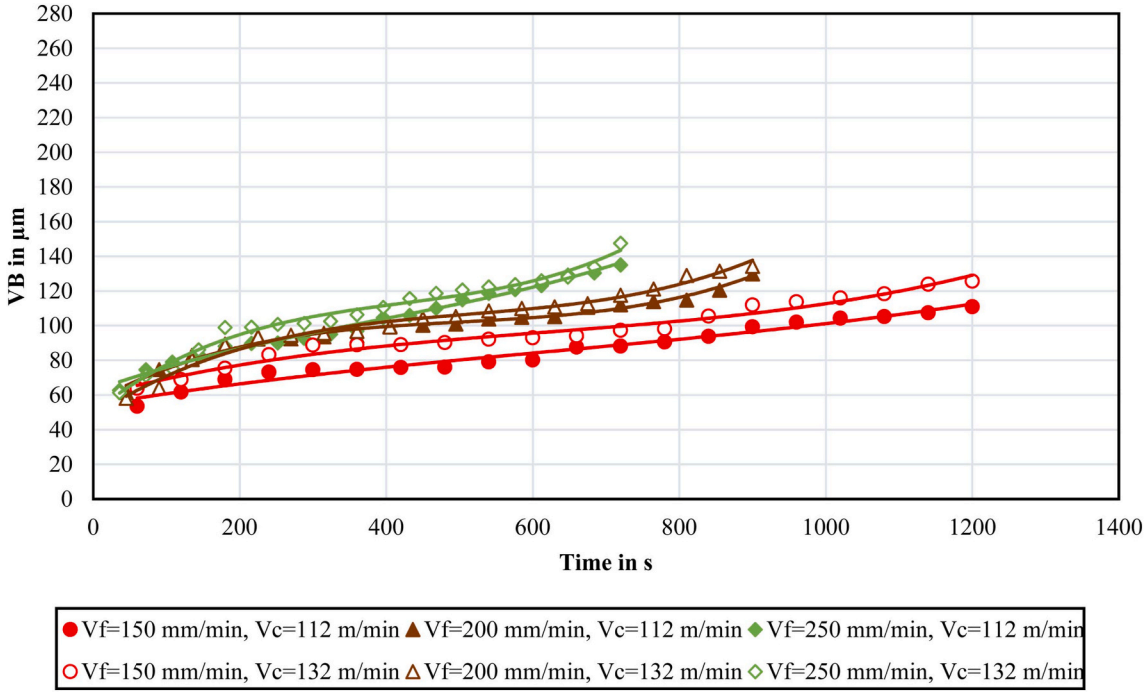

Fig. 9. Wear Progress for Flank face of uncoated tool.

The cutting force progression over time for both **TiN-coated** and **uncoated tools** is shown in Figs. 10 and 11, respectively. Several trends can be observed.

3.2.1. Coated tools exhibit lower cutting forces overall

At comparable cutting conditions, the TiN-coated tools consistently demonstrate **lower cutting forces** than their uncoated counterparts. For example.

- At $v_f = 250$ mm/min, $v_c = 132$ m/min, the maximum force measured with the coated tool remains **530 N**, while the uncoated tool exceeds **580 N** under the same conditions.
- Similarly, for $v_f = 150$ mm/min, $v_c = 112$ m/min. The coated tool maintains forces of 350 **N,** whereas the uncoated tool reaches up to **410 N.**

This reduction in force is attributed to the **lower friction coefficient** of the TiN coating and its ability to act as a thermal barrier, which helps maintain the hardness and structural integrity of the cutting edge under elevated temperatures [37].

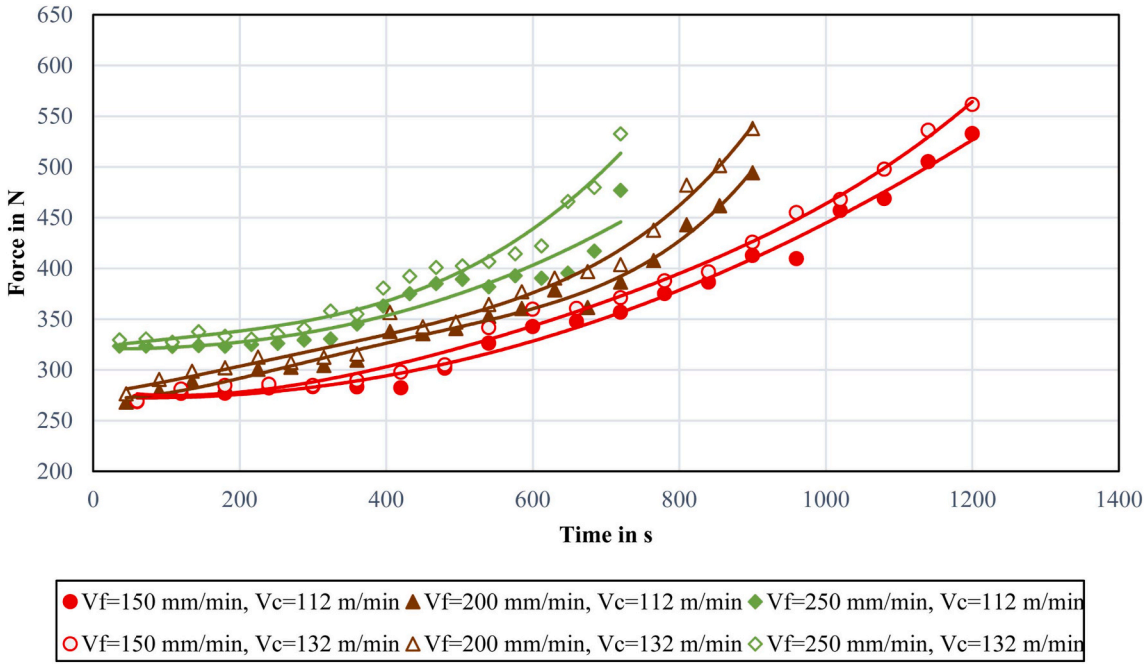

Fig. 10. Cutting force progression for coated tool.

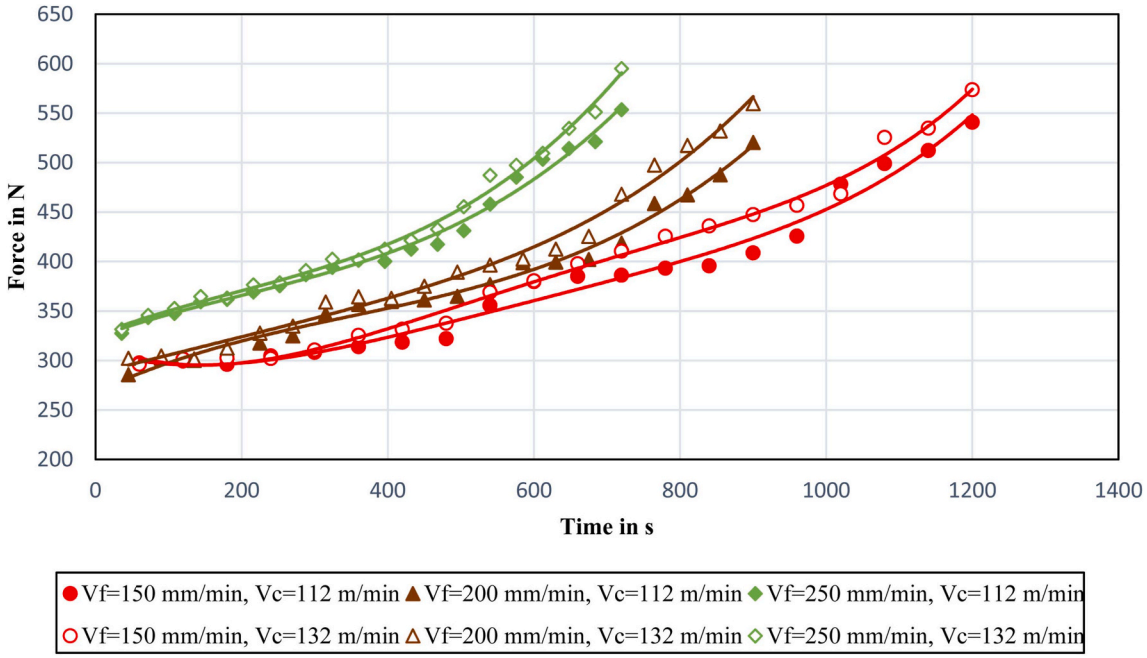

Fig. 11. Cutting force progression for uncoated tool.

3.2.2. Cutting force increases over time with tool wear

In both tool types, cutting force increases progressively as machining time advances. This trend correlates with the previously observed wear behavior.

- **Progressive tool wear** leads to increased contact area, altered chip formation mechanics, and elevated friction at the tool–chip interface.
- The increase is more **pronounced for uncoated tools**, where flank and rake wear advance faster, resulting in a sharper force rise, particularly under high-load conditions.

3.2.3. Influence of cutting parameters

Higher feed speeds and cutting velocities generally result in **increases in cutting force**, regardless of coating.

- At high parameters like $v_f = 250\ \text{mm/min}, v_c = 132\ \text{m/min}$, both tool types show strong force growth trends.
- Conversely, lower settings such as $v_f = 150\ \text{mm/min}, v_c = 112\ \text{m/min}$ lead to **more stable and lower force curves**, especially for coated tools, where wear resistance delays the onset of edge degradation.

3.3. Simulation validation

To assess the reliability of the developed finite element model, the simulation results were validated against experimental data, focusing on cutting forces and chip geometry. The simulated cutting force components were compared with experimentally measured forces reported in earlier section 3.2. Both the magnitudes and trends showed strong agreement, indicating that the model effectively captures the mechanical behavior of the cutting process.

In addition to force validation, chip thickness predicted by the simulation was compared with measurements taken using a digital light microscope. For the case involving the TiN-coated tool, with a feed speed of 200 mm/min and a cutting velocity of 112 m/min, the maximum chip thickness observed experimentally was 72 μm, while the simulation predicted 78 μm - resulting in a deviation of roughly 8 %.

A visual comparison between the simulated chip shape and the measured chip profile is presented in Fig. 12. Fig. 12 (a) shows a FE model of the generated chip profile at a $v_f = 200$ mm/min, $v_c = 112$ m/min. The predicted chip thickness was around 78 μm. Fig. 12(b) shows the digital light microscopy image of the chip generated at the same machining parameters. Despite minor differences in edge curvature and local thickness, the overall agreement in maximum chip thickness (78 μm in simulation vs. 72 μm in experiment) confirms the validity of the simulation approach.

The level of discrepancy observed falls within the range typically accepted in cutting simulations. Previous studies have reported variations of up to 10 %, often attributed to idealized contact conditions, simplified thermal boundaries, and inherent limitations in mesh resolution or material property definitions [31]. Given these factors, the current results are considered accurate enough to support the extraction of thermal and tribological characteristics for use in wear prediction models. However, the progressive evolution of tool wear and its impact on forces and contact conditions are not simulated by the FEM itself. Instead, these aspects are captured empirically through time-series features of the measured force signals, which are correlated with tool wear in the machine learning prediction. The model thus learns the statistical relationship between physical features (from the as-new FEM model), process parameters, empirical force features, and observed wear, rather than deriving wear curves from a fully physics-based, incrementally updated simulation.

3.4. Model evaluation and comparative analysis

To evaluate the performance of the proposed Grey-Box machine learning framework for tool wear prediction, several model configurations were tested. The results, summarized in Table 5, include predictions for both KT and VB across different modelling strategies.

3.4.1. SVR without feature selection or hyperparameter tuning

This baseline model, using SVR, was trained on the full feature set without any selection or tuning. It produced the **poorest results**, with negative R^2 values for both rake and flank wear predictions, indicating performance **worse than a horizontal mean predictor**. Without feature filtering, the model likely incorporated noisy and irrelevant features that have little to no correlation with tool wear. The absence of hyperparameter tuning further weakened its ability to learn meaningful patterns from the data.

Table 5
Effect of feature selection and white-box integration on machine learning model performance for tool wear prediction.

	MAE (**Mean Absolute Error**)	RMSE (**Root Mean Squared Error**)	R^2 (**Coefficient of Determination**)
SVR without Hyperparameter (Rake wear prediction)	38,48	44,63	−0,018
SVR without Hyperparameter (Flank wear prediction)	14,67	19,14	−0.010
SVR with feature selection and Hyperparameter (Rake wear prediction)	7,85	12,88	0.915
SVR with feature selection and Hyperparameter (Flank wear prediction)	5,43	7,45	0,847
GBR with feature selection (Rake wear prediction)	3,24	7,42	0,953
GBR with feature selection (Flank wear prediction)	4,15	6,64	0,920
GBR with feature selection without features of white box (Rake wear prediction)	10,52	15,36	0,541
GBR with feature selection without features of white box (Flank wear prediction)	8,11	10,57	0,427

3.4.2. SVR with feature selection (ANOVA + WOA) and hyperparameter tuning

Applying ANOVA followed by WOA allowed the model to focus on the most relevant physical and statistical features. With hyperparameter optimization, SVR performance improved dramatically: R^2 reached **0.915 for rake wear** and **0.847 for flank wear**, with significantly lower MAE and RMSE values. This configuration benefits from both feature selection (removing irrelevant features) and fine-tuned model behavior, allowing SVR to generalize well and capture wear progression trends.

3.4.3. GBR with feature selection

Switching to Gradient Boosting further improved predictive accuracy. The model reached $\mathbf{R^2 = 0.953}$ **for rake wear** and **0.920 for flank wear**, with MAE values of just **3.24** and **4.15**, respectively. Gradient Boosting effectively handles non-linear feature interactions and benefits from ensemble learning, making it well-suited for complex, multi-

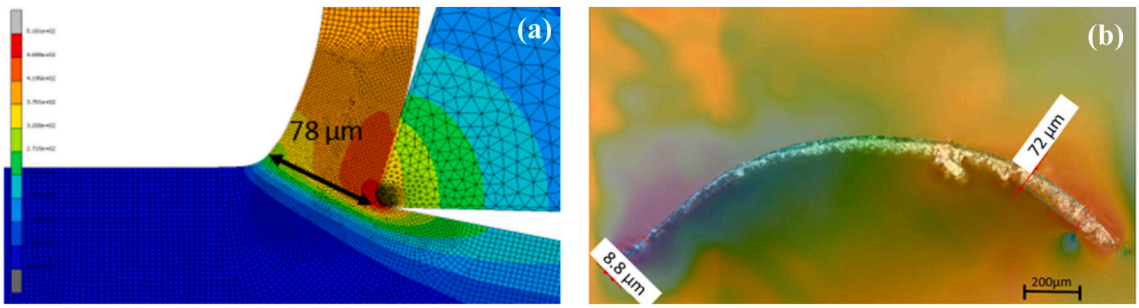

Fig. 12. Comparison of chip thickness from (a) FE simulation results and (b) digital light microscope measurements for the TiN-coated tool, at a v_f of 200 mm/min and $v_c = 112\ m/min$.

dimensional data such as force, vibration, and simulation features.

3.4.4. GBR without White-Box features

To evaluate the impact of simulation-derived (White-Box) features, a version of the GBR model was trained using only process and time-series features. R^2 dropped from **0.953 to 0.541** for rake wear and from **0.920 to 0.427** for flank wear. Omitting White-Box features such as relative sliding velocity or maximum interface temperature significantly reduces the model's understanding of the physics behind the wear of tools. This confirms that incorporating finite element simulation outputs enhances both accuracy and interpretability.

3.5. Correlation analysis

To further interpret the selected features and assess their relationships with tool wear, a correlation matrix was computed for the WOA-selected inputs and the target variable Wear_rake (due to a large number of features, only some selected features are shown for the correlation matrix). As shown in Fig. 13, rake wear exhibits a strong positive correlation with both the preset process parameter and the resulting process response (cutting force), highlighting the relevance of both input settings and their physical effects during machining. Moderate correlations are also observed with temperature at the tool–chip interface and the relative sliding velocity at the rake face. This analysis provides insight into the physical relevance of selected features and supports the explanation for the Grey-Box model.

The correlation analysis clarifies the physical relevance of selected features. Feed speed and cutting velocity directly impact cutting forces and temperatures, leading to increased wear rates as mechanical and thermal loads increase. The positive correlation of maximum interface temperature and relative sliding velocity with tool wear corroborates their roles in accelerating diffusion and adhesive wear mechanisms, consistent with established tribological theory [18,21]. Similarly, force-based features such as elevated crest factors indicate transient spikes in load that coincide with micro-fracturing or coating delamination events, linking signal dynamics to tool degradation pathways.

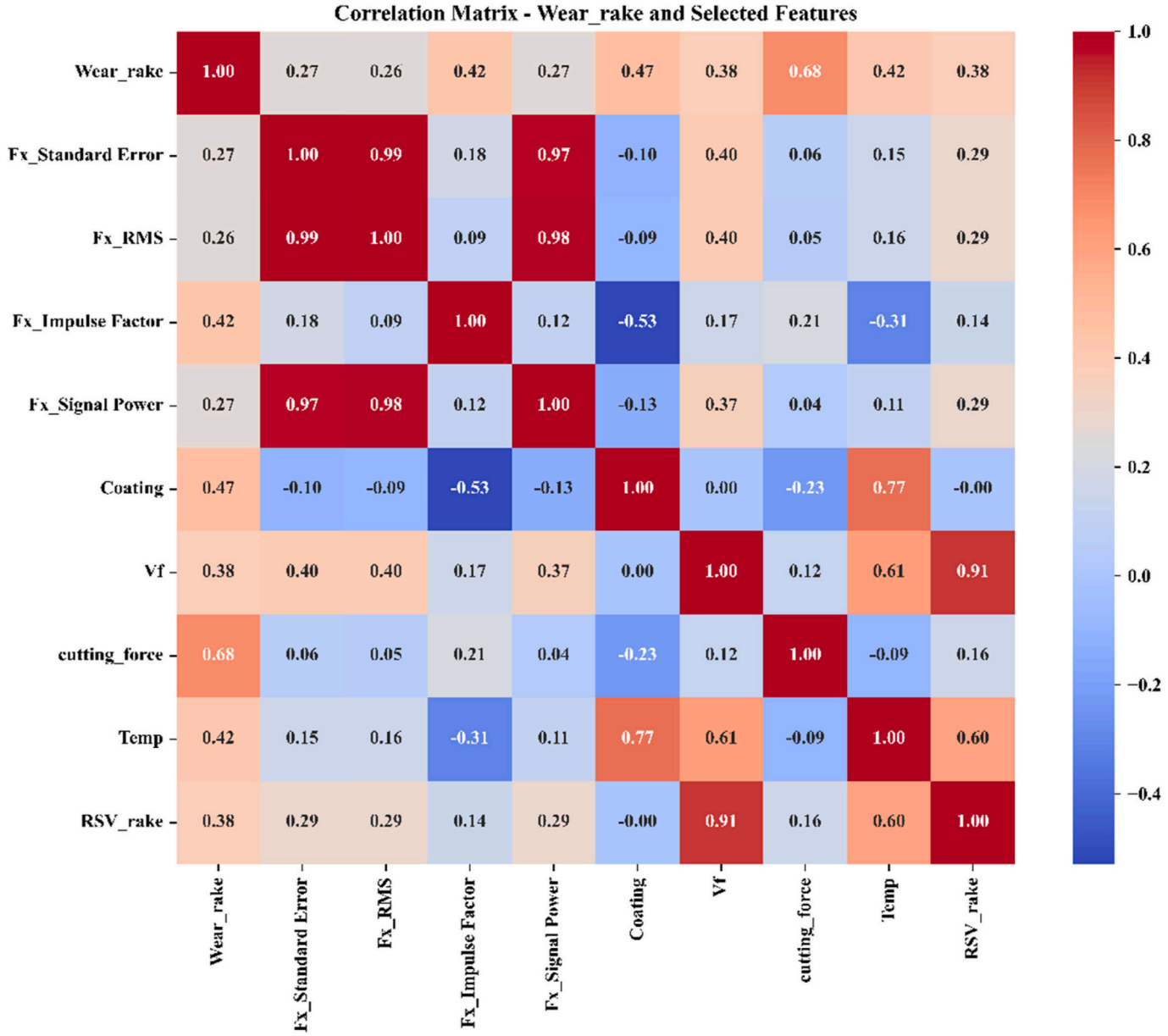

Fig. 13. Correlation matrix showing the relationships between rake face wear and the selected input features from the WOA-optimized model.

3.6. Model generalization on unseen test cases

To evaluate the generalizability of the trained GBR model, two experimental conditions excluded from the training phase were used as test cases.

1. **TiN-coated tool** at $v_f = 250$ mm/min, $v_c = 132$ m/min
2. **Uncoated tool** at $v_f = 150$ mm/min, $v_c = 112$ m/min

The model was applied to predict both **VB** and **KT** for these conditions, and the results were compared to experimentally measured values. The comparisons are visualized in Figs. 14 and 15, where the relative wear prediction error is plotted alongside the experimentally measured values for each sample.

3.6.1. Prediction performance: uncoated tool

For the uncoated tool, the model still achieved **reasonably accurate predictions**, though with slightly **larger deviations** in the early stages of the wear prediction (Fig. 14), for both flank and rake faces. The predicted values remain close to the actual trend but slightly **underestimate** wear in the samples at later stages. This deviation may stem from the **higher variability** and more abrupt wear behavior of uncoated tools, where micro-fractures and built-up edge formation are more prominent and harder to model purely from averaged features.

3.6.2. Prediction performance: coated tool

For the TiN-coated tool, the GBR model demonstrated **high prediction accuracy** for both wear types. The predicted value shows high variation for wear at the rake face than at the flank face from the measured experimental values. There is a sweet spot for both the faces (rake and flank) where the predictions are very close to the experimentally measured values, 80–140 μm for the flank face and 100–170 μm for the rake face. This can be because of the stable wear progression at the mid stages, where wear follows predictable, linear trends (e.g., abrasive wear), which align well with time and frequency-domain features. However, the model shows slightly higher deviations at the beginning and end stages. At initial stages, the tool wear is subtle and often nonlinear, producing minimal measurable signals (e.g., small forces). With sparse data, models struggle to generalize patterns. Also, the coated tools undergo a brief "run-in" phase where surface asperities wear off, causing transient thermomechanical behavior which is difficult to capture by various models. Whereas, the end stages involve coating delamination, substrate exposure, and accelerated degradation. The high wear at the end stage also introduces erratic signals (e.g., vibration spikes, force fluctuations) that mask underlying trends, thereby confusing data-driven models.

This result reflects the strength of the Grey-Box model in integrating both simulation-based features (e.g., temperature, sliding velocity) and time-resolved force metrics, which collectively capture the underlying wear mechanisms in high-speed cutting scenarios.

4. Conclusion

This study presented a Grey-Box machine learning framework for predicting tool wear in milling processes by integrating White-Box features derived from FE simulations, process parameters, and dynamic force-based time-series data, with a Black-Box machine learning model to capture complex, data-driven relationships. Finite element simulations were used to extract meaningful thermomechanical features, including contact temperatures and relative sliding velocity at the tool–chip interface, while experimental tests provided force signals and wear measurements for both TiN-coated and uncoated tools under various cutting conditions.

A two-stage feature selection process combining ANOVA and the Whale Optimization Algorithm (WOA) enabled the identification of the most relevant inputs for predicting rake and flank wear. Among the tested models, the GBR-enhanced by WOA-based feature filtering demonstrated superior predictive accuracy, achieving R^2 values above 0.95 for rake wear and 0.92 for flank wear. The inclusion of White-Box features significantly improved model generalization and interpretability, as demonstrated by strong performance on unseen test cases.

The results highlight the importance of combining physical insight with data-driven modelling to improve wear prediction in complex machining scenarios advancing beyond purely Black-Box models. This physically informed feature set enables the machine learning model to capture complex wear phenomena in milling while maintaining

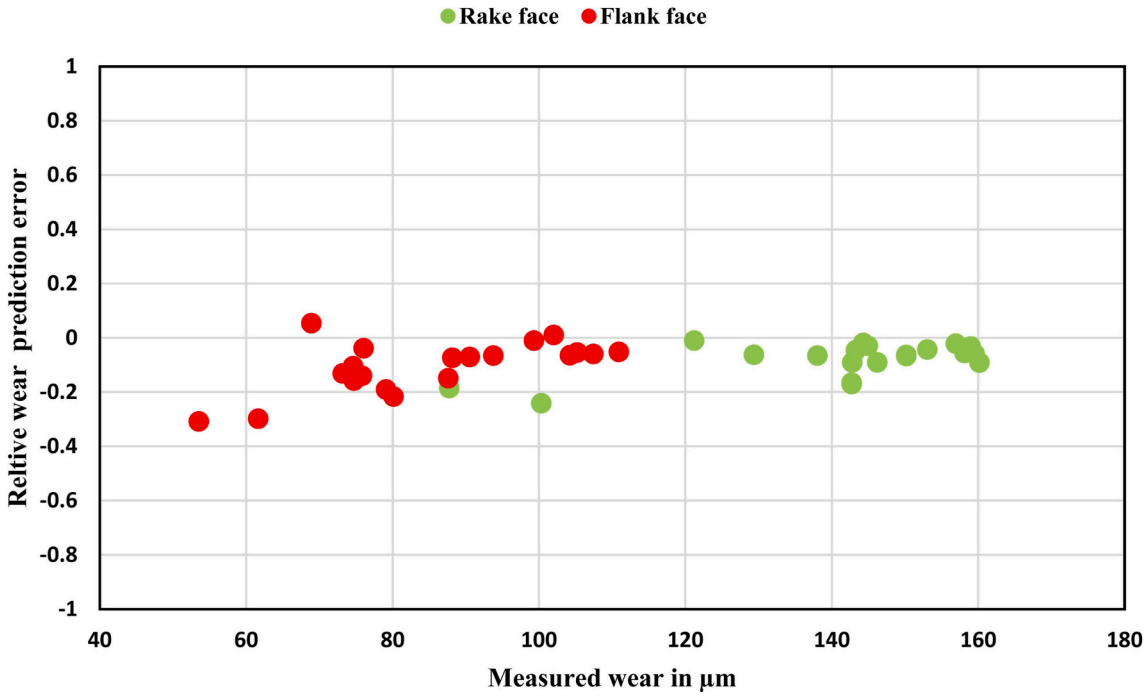

Fig. 14. Relative wear prediction error and measured values of flank and rake wear for uncoated tool.

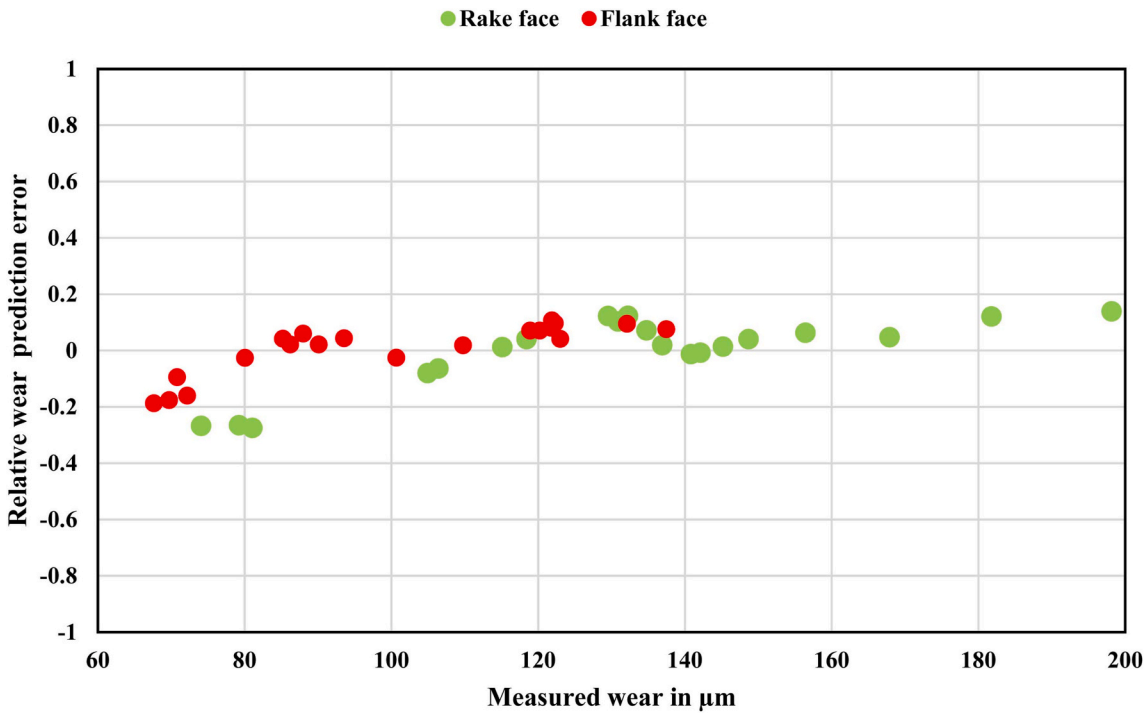

Fig. 15. Relative wear prediction error and measured values of flank and rake wear for TiN-coated tool.

transparency and relevance to manufacturing processes. Therefore, the proposed Grey-Box approach offers a promising path toward intelligent tool condition monitoring and process optimization in high-speed milling operations.

5. Outlook

While the proposed framework shows strong predictive performance and generalization, several limitations must be acknowledged:

Influence of lubrication: The experimental and simulation data were collected under dry machining conditions. The model may require retraining or adjustment for processes involving lubrication or coolant, which influence heat transfer and wear mechanisms.

The number of process parameter combinations is limited (12). This is a common constraint in manufacturing studies due to high experimental cost and time. Although, the present dataset is sufficient for proof-of-concept and for quantifying the benefits of simulation-informed "grey-box" modelling, but broader generalizability (to new materials, tool geometries, additional process parameters) will require more experimental and simulation data. This study is only focused on a single workpiece material (AISI 1045 steel) and two tool types (TiN-coated and uncoated carbide).

Offline feature extraction: Although time-resolved features were used, all data processing was performed offline. Real-time implementation would require embedded signal processing and computational efficiency enhancements.

Future work will focus on extending the Grey-Box approach to real-time wear monitoring, integrating additional sensors (e.g., temperature, acoustic emission), and testing across a wider range of machining setups. The physical fidelity of the framework can also be improved by incorporating iterative 3D FEM simulations that periodically update tool geometry to reflect wear progression. This would enable direct simulation of evolving contact conditions, potentially improving prediction accuracy and physical interpretability Moreover, the inclusion of wear-resistant coatings with different thermal and mechanical properties can help generalize the model for broader industrial applications.

CRediT authorship contribution statement

Amirmohammad Jamali: Conceptualization, Methodology, Investigation, Writing – original draft. **Amod Kashyap:** Conceptualization, Investigation, Resources, Writing – review & editing. **Johannes Schneider:** Resources, Visualization, Writing – review & editing, Supervision. **Michael Stuber:** Resources, Visualization, Writing – review & editing, Supervision. **Volker Schulze:** Conceptualization, Resources, Writing – review & editing, Supervision.

Declaration of generative AI and AI-assisted technologies in the writing process

During the preparation of this work the author(s) used DeepL in order to fix the grammatical mistakes and improve the readability of the manuscript. After using this tool/service, the author(s) reviewed and edited the content as needed and take(s) full responsibility for the content of the publication.

Declaration of competing interest

The authors declare that they have no known competing financial interests or personal relationships that could have appeared to influence the work reported in this paper.

Acknowledgement

The research work is funded under **SPP 2402: Greybox models for the qualification of coated tools for high-performance machining** project of Deutsche Forschungsgemeinschaft/German Research Foundation **(DFG).**

Data availability

Data will be made available on request.

References

[1] M. Storchak, H.C. Möhring, T. Stehle, Improving the friction model for the simulation of cutting processes, Tribol. Int. 167 (2022) 107376.
[2] G. Wang, M. Wang, P. Gao, B. Yang, Online tool wear prediction based on cutting force coefficients identification using neural network, Int. J. Adv. Des. Manuf. Technol. 136 (2025) 5153–5173.
[3] M.S.I. Chowdhury, B. Bose, K. Yamamoto, L.S. Shuster, J. Paiva, G.S. Fox-Rabinovich, S.C. Veldhuis, Wear performance investigation of PVD coated and uncoated carbide tools during high-speed machining of TiAl6V4 aerospace alloy, Wear 446–447 (2020) 203168.
[4] K. Ramasubramanian, N. Arunachalam, M.S. Ramachandra Rao, Wear performance of nano-engineered boron doped graded layer CVD diamond coated cutting tool for machining of Al-SiC MMC, Wear (2019) 1536–1547 (426–427), Part B.
[5] G. Chryssolouris, G. Chryssolouris, Overview of machining processes, Laser Machining: Theor. Pract. (1991) 1–16.
[6] K. Zhuang, K. Zhu, X. Wei, C. Hu, Z. Liu, Z. Gao, A dual-stage wear rate model based on wear mechanisms analysis during cutting Inconel 718 with TiAlN coated tools, J. Manuf. Process. 126 (2024) 24–34.
[7] A. Jamali, V. Schulze, Prediction of cutting tool condition in milling using optimization and non-optimization techniques, Proced. CIRP 133 (2025) 78–83.
[8] A. Mohamed, M. Hassan, R. M'Saoubi, H. Attia, Tool condition monitoring for high-performance machining systems—A review, Sensors 22 (6) (2022) 2206.
[9] K. Worden, G. Manson, The application of machine learning to structural health monitoring, Philos. Trans. R. Soc. A Math. Phys. Eng. Sci. 365 (1851) (2007) 515–537.
[10] D. Goyal, A. Saini, S.S. Dhami, B.S. Pabla, Intelligent predictive maintenance of dynamic systems using condition monitoring and signal processing techniques—A review, in: IEEE International Conference on Advances in Computing, Communication, & Automation, 2016, pp. 1–6.
[11] M. Saoubi, J.C. Outeiro, H.O.W.D. Chandrasekaran, O.W. Dillon Jr., I.S. Jawahir, A review of surface integrity in machining and its impact on functional performance and life of machined products, Int. J. Sustain. Manuf. 1 (1–2) (2008) 203–236.
[12] J. Wang, Y. Li, R.X. Gao, F. Zhang, Hybrid physics-based and data-driven models for smart manufacturing: modelling, simulation, and explainability, J. Manuf. Syst. 63 (2022) 381–391.
[13] H. Zhang, S. Jiang, D. Gao, Y. Sun, W. Bai, A review of physics-based, data-driven, and hybrid models for tool wear monitoring, Machines 12 (12) (2024) 833.
[14] M. Binder, F. Klocke, D. Lung, Tool wear simulation of complex shaped coated cutting tools, Wear 330 (2015) 600–607.
[15] Y.M. Arisoy, T. Özel, Machine learning based predictive modeling of machining induced microhardness and grain size in Ti–6Al–4V alloy, Mater. Manuf. Process. 30 (4) (2015) 425–433.
[16] B. Peng, T. Bergs, D. Schraknepper, F. Klocke, B. Döbbeler, A hybrid approach using machine learning to predict the cutting forces under consideration of the tool wear, Proced. CIRP 82 (2019) 302–307.
[17] L. Colantonio, L. Equeter, P. Dehombreux, F. Ducobu, A systematic literature review of cutting tool wear monitoring in turning by using artificial intelligence techniques, Machines 9 (12) (2021) 351.
[18] J. Schneider, S. Ulrich, J. Patscheider, M. Stueber, Wear study of a magnetron-sputtered TiC/aC nanocomposite coating under media-lubricated oscillating sliding conditions, Coatings 12 (4) (2022) 446.
[19] M. Stüber, H. Leiste, S. Ulrich, H. Holleck, D. Schild, Microstructure and properties of low friction TiC C nanocomposite coatings deposited by magnetron sputtering, Surf. Coating. Technol. 150 (2–3) (2002) 218–226.
[20] Aharon Inspektor, A. Paul, Salvador, architecture of PVD coatings for metal cutting applications: a review, Surf. Coating. Technol. 257 (2014) 138–153.
[21] K. Bobzin, C. Kalscheuer, M. Tayyab, Cracking behavior of wear resistant TiAlCrSiN coated cemented carbide compounds. Wear, 2025 205810.
[22] B. Shi, H. Attia, Current status and future direction in the numerical modeling and simulation of machining processes: a critical literature review, Mach. Sci. Technol. 14 (2) (2010) 149–188.
[23] M. Lotfi, S. Amini, M. Aghaei, 3D FEM simulation of tool wear in ultrasonic assisted rotary turning, Ultrasonics 88 (2018) 106–114.
[24] A. Attanasio, D. Umbrello, Abrasive and diffusive tool wear FEM simulation, Int. J. Material Form. 2 (2009) 543–546.
[25] R. Teti, K. Jemielniak, G. O'Donnell, D. Dornfeld, Advanced monitoring of machining operations, CIRP Ann. - Manuf. Technol. 59 (2) (2010) 717–739.
[26] M. Nouioua, M.L. Bouhalais, Vibration-based tool wear monitoring using artificial neural networks fed by spectral centroid indicator and RMS of CEEMDAN modes, Int. J. Adv. Des. Manuf. Technol. 115 (9) (2021) 3149–3161.
[27] H. Liu, Z. Liu, W. Jia, D. Zhang, Q. Wang, J. Tan, Tool wear estimation using a CNN-transformer model with semi-supervised learning, Meas. Sci. Technol. 32 (12) (2021) 125010.
[28] L. Ma, N. Zhang, J. Zhao, H. Kong, An end-to-end deep learning approach for tool wear condition monitoring, Int. J. Adv. Des. Manuf. Technol. 133 (5) (2024) 2907–2920.
[29] B. Stampfer, G. González, E. Segebade, M. Gerstenmeyer, V. Schulze, Material parameter optimization for orthogonal cutting simulations of AISI4140 at various tempering conditions, Proced. CIRP 102 (2021) 198–203.
[30] A. Svoboda, D. Wedberg, L.E. Lindgren, Simulation of metal cutting using a physically based plasticity model, Model. Simulat. Mater. Sci. Eng. 18 (7) (2010) 075005.
[31] T. Özel, The influence of friction models on finite element simulations of machining, Int. J. Mach. Tool Manufact. 46 (5) (2006) 518–530.
[32] G. Shi, X. Deng, C. Shet, A finite element study of the effect of friction in orthogonal metal cutting, Finite Elem. Anal. Des. 38 (9) (2002) 863–883.
[33] Florian Sauer, Amartya Mukherjee, Volker Schulze, Insights into the metal cutting contact zone through automation and multivariate regression modelling under the framework of gear skiving, Simulat. Model. Pract. Theor. 142 (2025) 103107.
[34] F. Akbar, P.T. Mativenga, M.A. Sheikh, On the heat partition properties of (TiAl)N compared with TiN coating in high speed machining, Proc. IME B J. Eng. Manufact. 223 (4) (2009) 363–375.
[35] H. Holey, F. Sauer, P.B. Ganta, L. Mayrhofer, M. Dienwiebel, V. Schulze, M. Moseler, Multiscale parametrization of a friction model for metal cutting using contact mechanics, atomistic simulations, and experiments, Tribol. Lett. 72 (4) (2024) 113.
[36] E. Usui, T. Shirakashi, T. Kitagawa, Analytical prediction of cutting tool wear, Wear 100 (1–3) (1984) 129–151.
[37] N.P.V. Sebbe, F. Fernandes, F.J. Silva, V.F. Sousa, R.C.M. Sales-Contini, R. D. Campilho, A.F.V. Pedroso, Wear behavior analysis of TiN/TiAlN coated tools in milling of Inconel 718, in: International Conference on Flexible Automation and Intelligent Manufacturing, Springer Nature Switzerland, Cham, 2023, June, pp. 784–795.